Advanced Structured Materials

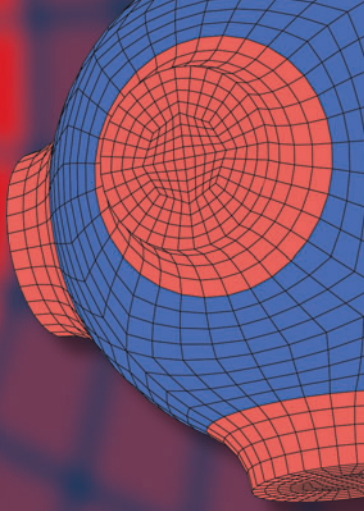

Zishan Husain Khan *Editor*

Recent Trends in Nanomaterials

Synthesis and Properties

Springer

Advanced Structured Materials

Volume 83

More information about this series at http://www.springer.com/series/8611

Zishan Husain Khan
Editor

Recent Trends in Nanomaterials

Synthesis and Properties

Springer

Editor
Zishan Husain Khan
Department of Applied Sciences
and Humanities
Jamia Millia Islamia
New Delhi, Delhi
India

ISSN 1869-8433 ISSN 1869-8441 (electronic)
Advanced Structured Materials
ISBN 978-981-10-3841-9 ISBN 978-981-10-3842-6 (eBook)
DOI 10.1007/978-981-10-3842-6

Library of Congress Control Number: 2017935822

Printed on acid-free paper

This Springer imprint is published by Springer Nature
The registered company is Springer Nature Singapore Pte Ltd.
The registered company address is: 152 Beach Road, #21-01/04 Gateway East, Singapore 189721, Singapore

Foreword

Since the announcement of the establishment of the US National Nanotechnology Initiative (NNI) in the year 2000 by President William Jefferson Clinton, NNI-supported research and development is producing many scientific and technological innovations. The initiative has spawned many countries around the world to invest in their own nanotechnology initiatives that have led to the invention and commercialization of products that are used every day in consumer products that will make our lives more productive and sustainable. Nanotechnology is pervasive in many different areas such as energy, health, materials, electronic devices, advanced manufacturing, computing, and related technologies. Nanotechnology-based electronics are making devices smaller and faster and are developing alternative fuel sources that will eventually replace the use of fossil fuels. Nanoscale understanding provides researchers the unique ability to diagnose diseases and to target bespoke treatments, thereby increasing the chances of a longer life. Manufacturing issues such as scalability, reliability, and cost are critical for nanotechnology products to live up to our expectations. Nanotechnology research has also led to the development of materials that are lighter, stronger, and more resistant to damage when compared to traditional materials. These achievements have been driven by scientific curiosity, demand, and financial support by Government agencies and multinational corporations.

The future holds great promise for new and disruptive innovations that are not possible without the properties that exist at the nanoscale. The ability to control and manipulate information, multifunctional and self-healing structures, energy-scavenging technologies, personalized medicine, and many other inventions have yet to be discovered. This book is intended to inform the reader of the current state of the art in nanomaterials and their applications. I salute Prof. Zishan Husain Khan for compiling such a collection of very well-written and informed chapters associated with current thinking and understanding of using and developing nanomaterials. Chapter 1 presents a review of the research work reported on the synthesis and characterization of graphene oxide and the challenges still facing scientists in perfecting this material. Chapter 2 focuses on the wear of nanocomposites, its mechanisms, types, and analysis of wear debris. Wear behavior of metals, ceramics,

and polymers is also described along with a special focus on iron-alumina metal matrix nanocomposites and a mechanism to reduce the overall wear rate in any system. Chapter 3 is mainly focused on the targeted drug delivery using nanoparticles. The mechanism of action of targeted delivery is discussed in detail with the applications of different types of nanoparticles in targeted delivery. This chapter also explains the synthetic procedures of producing nanoparticles for use in targeted drug delivery. Chapter 4 describes the application of graphene quantum dots used in the fields of biomedicine, biosensing, optoelectronics, and energy conversion and storage. Chapter 5 presents an overview of progress made in the fabrication of hybrid nanostructured transparent conductive film (TCF) based on the assembly of one-dimensional metal nanowires and two-dimensional graphene films. The concept of nanostructured hybrid films is expected to open up possibilities for developing next-generation TCF with multiple functionalities. Chapter 6 illustrates the antibacterial properties of nanoscale materials and describes the effect of pure and doped ZnO nanoparticles on the antibacterial activity against two Gram-negative *Escherichia coli* and *Pseudomonas aeroginosa* and two Gram-positive *Bacillus subtilis* and *Staphylococcus aureus* bacteria. Chapter 7 focuses on the synthesis of large area graphene in an affordable, non-toxic way. This chapter describes microwave-assisted synthesis of graphene and electrochemical exfoliation methods with applications in the fields of electro-magnetic shielding and field-effect transistors. Chapter 8 is aimed at understanding the recent progress in the development and characterization of a new group of nanomaterials, in freestanding forms, such as fiber/yarns, paper/sheet, and bulk forms of supply, which were derived from graphene nanosheets using various fabrication technologies. Chapter 9 illustrates how laser-assisted molecular beam epitaxy growth affects the properties of GaN nanowall networks for the improvement of products and devices. Chapter 10 provides a lucid description of the density functional theory of two- and three-dimensional networks, while the final chapter of the book provides an understanding of how nanostructured zirconium oxides (ZrO_2) have emerged as versatile and promising materials in the biomedical field due to their biocompatibility and excellent physicochemical properties. Readers of this volume are encouraged to throughly read and understand these informative chapters in the hope of stimulating further research in the exciting field of nanotechnology.

I wish to thank all the contributing authors of this volume who have provided a wide scope of knowledge in the area of nanomaterials. I also wish to thank and acknowledge the efforts of Prof. Zishan Husain Khan for his knowledge and ability to compile such a first-class book on the advanced in nanomaterials, and hope that experienced researchers and graduate students alike will use the book as a source of reference on nanomaterials in the years to come.

Prof. Mark J. Jackson, Ph.D., D.Sc.
McCune and Middlekauff Endowed Professor and Academic Program Leader
College of Technology and Aviation Kansas State University
Salina, KS, USA

Acknowledgements

First and foremost, I am thankful to God. In the process of putting this book together, I realized how true this gift of writing is for me. You have given me the power to believe in my passion and pursue my dreams. I could never have done this without the faith I have in you, the Almighty.

I would like to express my gratitude to all the authors for their significant contributions to this book. It would not have been possible to undertake this challenging work and enabling me to accomplish it without your support and timely response. All the authors have justified their contribution in this book by presenting the work on latest areas of nanomaterials and their applications. I owe them a lot.

I would like to thank Prof. Talat Ahmad, Vice-Chancellor, Jamia Millia Islamia, New Delhi (India), for his ongoing support and encouragement for creating an academic environment in the pursuit of higher education. His pearls of wisdom coupled with motivation have contributed largely to the completion of this book.

I would like to express my gratitude to Prof. Mushahid Husain, Vice-Chancellor, MJP Rohilkhand University, Bareilly (Uttar Pradesh), India, and Prof. Haroon Sajjad, Department of Geography, Jamia Millia Islamia, New Delhi (India), for their valuable suggestions and motivation during the compilation of this book. I admire their distinguished helping nature.

I am grateful to all who saw me through this book and to all those who provided support, talked things over, read, wrote, offered comments, and assisted in the editing, proofreading, and design. My thanks are due to all of Ph.D. students especially Mohd. Bilal Khan, Mohd. Parvaz, and Sutan Ahmad, who helped me a lot in completing this work.

I would also like to acknowledge the support and guidance provided by the editorial team of Springer without whom this endeavor would not have been a reality.

Last but not least, my deepest gratitude goes to my family for their unflagging love and support throughout the process of compilation of this book. They have been a constant source of inspiration and I dedicate this book to them. I am also indebted to my mother for her encouragement and allowing me to follow my

ambitions throughout my childhood. I am grateful to my wife Rubina Mirza for her constant support and for standing beside me throughout my career. She has been my inspiration and motivation for continuing to improve my knowledge and move my career forward. I also thank my wonderful children Ayanab, Alina, and Ali for always making me smile and for understanding on those weekend mornings when I was working on this book instead of playing games with them. I hope that one day they can read this book and understand why I spent so much time in front of my computer.

As an editor, I would love to receive suggestions and feedback for the book at zishan_hk@yahoo.co.in.

Contents

at King Abdul Aziz University, Jeddah, Saudi Arabia, in 2007. Dr. Khan worked as an associate professor at this center until July 2012. During his stay there, he established the world-class facilities in nanotechnology with clean room of level 100. He also was actively involved in designing various courses in nanotechnology. He also acted as a reviewer for many international journals of high repute. In addition, he has edited several special issues for reputed international journals. Dr. Khan has edited two books entitled "*Recent Trends in Nanotechnology & Renewable Energy*" published by Bharti Publications, Delhi (India), and "*Advances in Nanomaterials*" published by **Springer**.

Chapter 5
Graphene/Metal Nanowire Hybrid Transparent Conductive Films

Iskandar Kholmanov, Giorgio Sberveglieri and Muhammad A. Alam

5.1 Introduction

Transparent conductive films (TCFs) are attracting significant interest due to their potential applications in a broad range of emerging device technologies. As a result, a new generation of TCF materials has been proposed [1, 2]. Figure 5.1 illustrates different types of thin films for TCF applications. Among the metal oxide films, indium tin oxide (ITO) is a mature technology and is widely used in various devices/systems. Other oxides, such as fluorine-doped tin oxide (FTO) and aluminum-doped zinc oxide (AZO) are used for specialized devices. ITO (or tin doped indium oxide) is a heavily doped n-type semiconductor with a bandgap of 4 eV. Doping increases electrical conductivity, while the wide bandgap provides the high transparency in the visible range of the spectrum needed for this class of devices [3]. However, the poor compatibility with organic materials, opaqueness to the infrared spectra, brittle ceramic structure and the uncertain availability of indium are some of the key challenges for the use of ITO films in TCFs applications, particularly in flexible and large area optoelectronic devices [2]. Moreover, it is known that indium can diffuse into the functional layers of organic photovoltaic (OPV) devices and organic light emitting diodes (OLEDs) [4, 5], introducing recombination centers that degrade device performance. These drawbacks of ITO

I. Kholmanov (✉)
Department of Mechanical Engineering, The University of Texas at Austin, Austin, TX 78712, USA
e-mail: iskandar.kholmanov@ino.it

I. Kholmanov · G. Sberveglieri
CNR-INO, Sensor Lab, The University of Brescia, via Branze 45, 25123 Brescia, Italy

M.A. Alam
School of Electrical and Computer Engineering and Birck Nanotechnology Center, Purdue University, West Lafayette, IN 47907, USA

Z.H. Khan (ed.), *Recent Trends in Nanomaterials*,
Advanced Structured Materials 83, DOI 10.1007/978-981-10-3842-6_5

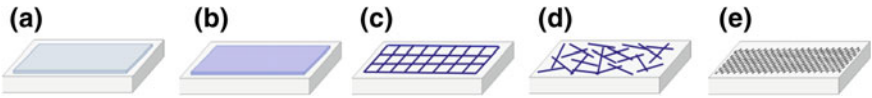

Fig. 5.1 An illustration of transparent conductive films composed of different materials: **a** ITO metal oxide, **b** conductive polymer, **c** periodic metal grid, **d** percolated random network of one-dimensional nanostructures, such as carbon nanotubes and metal nanowires, and **e** two-dimensional graphene

have stimulated intensive research in developing new materials that can meet the evolving requirements of the TCF market. For example, several other materials including conductive polymers, metal grids, metal nanowires (NWs), carbon nanotubes (CNTs) and graphene-based films have been investigated as alternatives to ITO (Fig. 5.1).

Conductive polymers, such as poly(3,4-ethylenedioxythiophene) polystyrene sulfonate (PEDOT:PSS) have a great potential to replace ITO for TCF applications. Conductive polymer films are inexpensive, mechanically flexible, and involves environmentally benign processing. However, their degradation under photochemical, thermal, oxidative, and mechanical processes limits their applications in a broad range of optoelectronic devices [6, 7].

Fully interconnected, periodic metal grid films offers high electrical conductivity [8], and the optical transparency of these films can be tuned by the geometry and density of the grid structure on the substrate surface. The lithographically-defined metal grid TCFs, however, are expensive, unsuited for applications in large area systems. In addition, the effect of chemical reactivity of metals on other functional parts of the devices is not yet fully investigated.

Nanostructured films based on percolated random network of one-dimensional (1D) metal nanowires (NWs) and CNTs, and continuous two-dimensional (2D) graphene conductive films are considered as promising alternatives to ITO because of their unique physical and chemical properties [1, 2]. Percolated and randomly oriented metal NW films, for example, have sheet resistance (R_s) and optical transmittance (T) comparable to/or better than ITO films. Compared to metal grid films, the NW films can be obtained using relatively low-cost fabrication methods. However, the high surface roughness, poor adhesion to some substrates, and high chemical reactivity of metal NW films limit their long-term applications or make them incompatible with functional parts of certain devices.

CNT films often present good thermal and chemical stabilities and good optical and electromechanical characteristics. These properties make them promising for TCFs applications [9, 10]. The electrical conductivity of CNT films is provided by charge transfer through percolated networks of nanotubes. The one of the main drawbacks of these films is their relatively high sheet resistance (R_s), mainly contributed from the nanotube-nanotube junction resistance [11, 12].

2D graphene, a recent nanomaterial with prominent Optoelectrical characteristics, is considered as another alternative to ITO for TCFs applications. Theoretical values of charge carrier mobility in graphene can be as high as 200,000 cm^2/V s,

demonstrating its remarkable transport properties [13]. Additionally, single layer graphene absorbs about 2.3% of visible light [14, 15]. Combined, these superior properties make graphene an excellent candidate for TCF applications. In spite of theoretically predicted superior electrical conductivity, graphene-based films have relatively high sheet resistances. TCFs fabricated using chemically modified graphene have a sheet resistance $R_s > 5$ kΩ/sq with an optical transmittance lower than 90% at 550 nm wavelength (T_{550}) [16, 17]. Single layer graphene films grown by chemical vapor deposition (CVD) has a typical sheet resistance of about $R_s > 1$ kΩ/sq with optical transmittance of about $T_{550} = 97.5\%$ [18].

Current ongoing research investigations are focused on development of advanced strategies to address the key issues and to improve the performance of single component nanostructured TCFs discussed above. One of the prominent concepts is development of *hybrid nanostructured films*, in which the shortcomings of single component TCFs is overcome by the presence of another component, and the overall performance of the hybrid films is improved due to synergy between individual components [19–21]. This concept opens up possibilities for developing next generation multi-component and multi-functional TCFs.

Given this summary of the various single and multi-component TCFs, we now consider these systems in detail. We begin with a review of single component 2D graphene (Sect. 5.2) and 1D metal nanowire (Sect. 5.3) films, to provide a baseline for our discussion of the multicomponent hybrid TCFs composed of these two components. In Sect. 5.4, we describe the fabrication and characterization of optical and electrical properties of RG-O/Cu NW hybrid films, as well as the multi-functionality of RG-O platelets in the films. Section 5.5 focuses on the fabrication and characterization of CVD-graphene/Ag NW hybrid films. This section also considers the heat dissipation properties of the CVD-graphene layer that improve the thermal stability of the hybrid films. In Sect. 5.6, applications of graphene/metal nanowire hybrid TCFs in electrochromic devices are presented, highlighting the advantages of the hybrid films over the corresponding single component TCFs. Section 5.7 summarizes and briefly presents the future challenges of nanostructured hybrid TCFs.

5.2 Graphene-Based Transparent Conductive Films

First graphene-based transparent conductive films were fabricated using graphene oxide (G-O) platelets obtained by solution-based oxidation and exfoliation of graphite (modified Hummers method) [17, 22–24]. G-O can be dispersed in water and form stable colloidal aqueous suspension. G-O platelets are decorated with oxygen-containing functional groups (such as carboxyl, hydroxyl, epoxy) located at both sides of the basal plane and at the edges. The presence of these functional groups results in a poor electrical conductivity of G-O. Different reduction methods, such as thermal, chemical and electrochemical approaches have developed to remove the functional groups and restore the graphitic structure of the platelets.

To achieve highly reduced G-O films by thermal treatment high-temperatures (>1000 °C) and ultrahigh vacuum (or a reducing environment) are required [17, 23–25]. Chemical reduction involves reducing agents such as hydrazine, [17, 26–28] N,N-dimethyl hydrazine, [23] and sodium borohydride [29] and because of their toxic properties, safety precautions must be taken when large quantities of these reagents are used. Electrochemical reduction involves changing the Fermi energy level of the electrode material surface and thus direct charge transfer is used to efficiently reduce G-O films on the electrode surface [30, 31]. Ongoing research in this field is actively progressing, and recently developed new methods using metal foils or particles allows facile reducing of G-O at near-room temperatures [32–35].

The reduced graphene oxide (RG-O) possesses substantially higher electrical conductivity compared to that of G-O. Conductive RG-O films are fabricated either by reduction of pre-deposited G-O films, or by deposition of RG-O dispersions on a substrate. The first approach is widely used because G-O dispersions can be easily deposited on a various kind of substrates forming continuous thin G-O films and can be subsequently reduced to obtain RG-O films (Fig. 5.2a, b). Although the electrical properties of the RG-O strongly depend on the degree of reduction, none of the existing reduction methods allows fabrication of RG-O films with sheet resistance $R_s < 1$ kΩ/sq with $T_{550} > 90\%$. Such high sheet resistance is partially contributed by large amount of structural defects formed during the fabrication (oxidation, exfoliation, sonication) processes. The defects can scatter the charge carriers, adversely affecting the transport properties of the RG-O platelets. In addition, because of a limited lateral size of RG-O platelets (from several nanometers up to some tens of micrometers (Fig. 5.2a) the continuous large-area films are formed by interconnected (mostly overlapped) platelets. Because of random orientation and absence of perfect hexagonal bonds between interconnected platelets, the platelet-platelet junctions may significantly contribute to the sheet resistance of the RG-O films. Residual impurities of chemicals used during

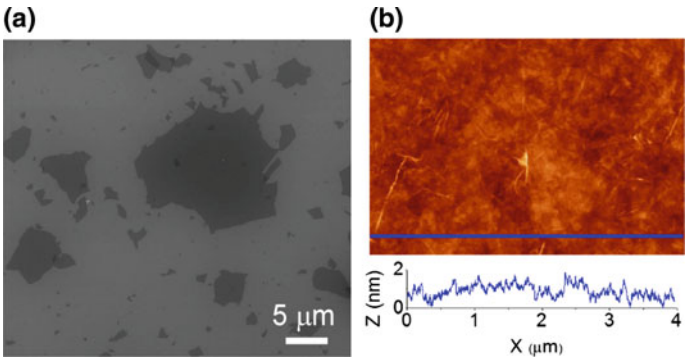

Fig. 5.2 **a** Scanning electron microscopy (SEM) image of RG-O platelets on a SiO_2/Si substrate. RG-O platelets with different sizes are shown. **b** Atomic force microscopy (AFM) image of thin RG-O films spin coated on a SiO_2/Si wafer. The line profile exhibits a relatively low surface of RG-O film. Reprinted with permission from [28]. Copyright 2013 American Chemical Society

solution-based oxidation exfoliation processes can also decrease the conductivity of RG-O films. These factors cannot be eliminated by the reduction processes and development of additional processing and treatments is required to restore the inherently high conductivity of graphene platelets.

In graphene grown by CVD of hydrocarbon gases on metal surfaces, the role of the factors adversely affecting the transport properties of the films, mentioned above for RGO films, is negligible. CVD growth method allows synthesizing of large-area single or few layer graphene films with structural qualities much higher than that of RG-O films [36, 37]. Due to these characteristics the potential of CVD-graphene for TCF applications is considerably higher compared to RG-O. However, typical monolayer CVD-graphene has a sheet resistance of about >1 kΩ/sq [18], markedly higher than that of ITO films. In addition, the charge carrier mobility in these CVD-graphene films is significantly lower [18] compared to that of mechanically exfoliated graphene [38] as well as theoretically calculated values [13]. The high sheet resistance of CVD-graphene films is contributed by different kind of defects formed during synthesis and transfer processes. Figure 5.3a shows a SEM image of a monolayer CVD-graphene grown on a polycrystalline Cu substrate. The graphene layer was grown continuously across the steps, facets and grain boundaries of the substrate. Different thermal contractions of the grown graphene layer and the metal substrate upon cooling yields line imperfections such as ripples and wrinkles, as observed in Fig. 5.3a [36]. Additional line disruptions are formed after the transfer of CVD-graphene onto SiO_2/Si substrates (Fig. 5.3b). These disruptions together with other structural defects, such as cracks, tears, point defects, etc., can scatter the charge carriers, adversely affecting charge carrier motilities and decreasing ballistic transport path lengths [13, 39, 40]. In addition, structurally CVD-graphene can be considered as a 1D polycrystalline layer with topological defects such as grain boundaries and crystal structure dislocations [41, 42]. Each graphene domain in CVD-graphene layer may have different crystallographic orientations, and the junctions between two neighboring domains form graphene grain boundaries.

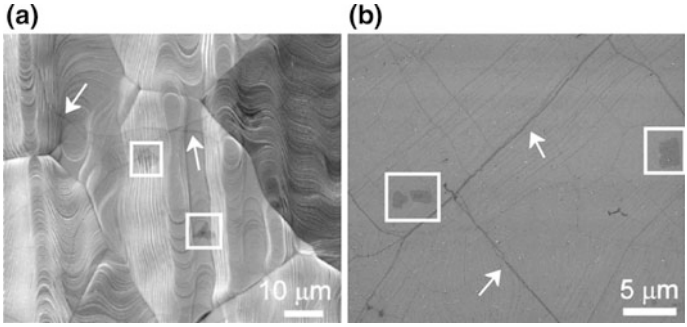

Fig. 5.3 SEM images of **a** CVD-graphene grown on a polycrystalline Cu substrate, and **b** CVD-graphene transferred onto a SiO_2/Si substrate. *Squared* areas contain dark islands that are bilayer CVD-graphene. *Arrows* indicate the line imperfections (folding, ripples and wrinkles) formed during the growth and/or transfer of CVD-graphene

These defects in graphene can essentially scatter the charge carriers and disturb the sp^2 delocalization of π electrons [41, 42]. Consequently the presence of such defects may lead to the low electrical conductivity decreasing the potential of CVD-graphene films for TCF applications.

Different approaches have been developed to minimize the role of defects and improve the electrical conductivity of CVD-graphene films. High temperature treatment to heal the structural defects, [43, 44] growing a larger grain size CVD-graphene to lower the density of grain boundaries [45], and various doping processes to increase the charge density [37] have been studied. However, to date these methods are yet to produce monolayer CVD-graphene films having a sheet resistance less than 100 Ω/sq that is required for many device applications.

In spite of above mentioned disadvantages, both RG-O and CVD-graphene are prominent candidate for next generation TCFs. One of the advantages of graphene-based films is their extremely low thicknesses (one-atom-thick for single layer graphene), compared to NW and CNT-based TCFs, and their 2D structure allows fabrication of continuous films. Another merit of graphene-based TCFs is their relatively high chemical stability that makes them consistent with functional components of diverse optoelectronic devices. Further research focused on development of new methods for production of less defective RG-O films, cost-effective fabrication, facile transfer and stable doping of CVD-graphene is needed in order to realize the full potential of graphene films for TCF applications, particularly, when they are used as a component in hybrid TCFs and provide additional functionalities, as described in the next sections.

5.3 Metal Nanowire-Based Transparent Conductive Films

Recently, thin films of percolated, randomly oriented metal NWs have received increased attention due to their excellent optical and electrical properties [2, 46, 47]. As other nanostructured films for TCF applications, metal NW films also exhibit good electromechanical performances retaining their stable electrical conductivity under mechanical strains. For practical applications mostly attractive metal nanowires are Cu (Fig. 5.4a) and Ag NWs (Fig. 5.4b) because of their relatively low-cost fabrication and good electrical conductivities [46, 47]. The NWs can be synthesized using simple wet-chemistry approaches, and large-area Ag and Cu NW transparent electrodes can be cheaply deposited using these NW solutions [46–48]. High optical transmittance in these mesh films is provided by open spaces between NWs, while good electrical conductivity is achieved due the percolated network of metal NWs. Therefore, optoelectrical properties of the films can be controlled by the density of the NWs in the film. Bottleneck in metal nanowires TCFs is NW–NW junction resistance. Mechanical pressing or heating of NW films can decrease the junction resistance, however, these processing might not be compatible with integrated devices. Recently developed plasmonic welding technique can substantially decrease the junction resistance between nanowires yielding metal NW

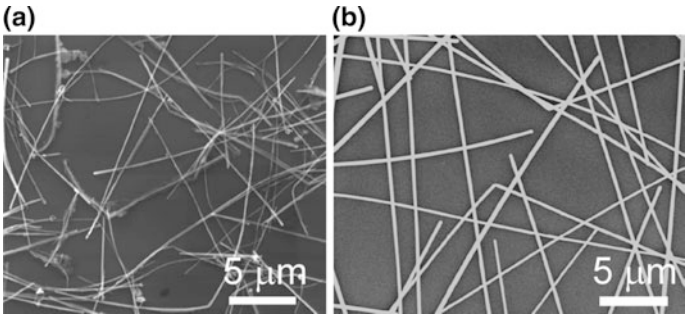

Fig. 5.4 SEM images of **a** Cu NWs with an average diameter less than 60 nm and average length longer than 20 μm (purchased from NanoForge), and **b** Ag NWs with an average diameter of 100–130 nm, and average length of 5–25 μm (purchased from SeaShell Technology) deposited onto SiO_2/Si substrate

films with a sheet resistance of 10 Ω/sq at 90% optical transmission [49]. Since this approach exclusively heats the NW–NW junctions, it can be used for NW films on plastic substrates without any damage. Another recent report has demonstrated the fabrication of metal nanotrough networks based on templating ultralong polymer nanofibers [50]. Because of the continuous network (absence of or very low electrical resistance at the nanotrough junctions), this approach allowed fabrication of metal nanotrough network films with a sheet resistance of 2 Ω/sq at 90% optical transmission.

Overall, in terms of optical transmittance and sheet resistance the metal NW films satisfy minimum application-specific requirements. However, large diameter (several tens of nanometers) as well as NW–NW junctions required for conductive network formation leads to undesirably increased surface roughness that can impede their applications in most of the sandwich-structured optoelectronic devices. In addition, metal NWs possess relatively high chemical reactivity. This may restrict the use of NW-based TCFs in certain optoelectronic devices in order to avoid the interaction (and subsequent degradation) of NWs with other active functional parts of devices. Moreover, at elevated temperatures the metal NWs transform into metal nanoparticle array that indicates the thermal instability of NWs [51]. Such instabilities may adversely affect the long term reliability of NW TCFs. Therefore, future research on the topic must address the chemical and thermal stabilities, optimization of structural and morphological characteristics, and compatibility of NWs with diverse device components.

The drawbacks of single component nanostructured transparent electrodes, such as graphene and NW films, can be minimized/eliminated in the hybrid films where shortcomings of one component are overcome by the second component, a concept originally proposed theoretically by Alam group at Purdue [19]. To date, various multi-component TCFs composed of two or more of the following structures: CNTs, metal NWs, metal grids, graphene, graphene oxide and conductive polymers, have been reported. Among these multi-component films, the hybrids of 2D graphenic

structures with 1D metal NWs are one of the most attractive ones, and therefore, here, we will discuss RG-O/Cu NW films (in Sect. 5.4), and CVD-graphene/Ag NW films (in Sect. 5.5).

5.4 RG-O/Cu NW Hybrid Transparent Conductive Films

Assembling of RG-O with Cu metal NWs is a promising strategy to overcome the drawbacks of the single component RG-O and Cu NW films. For preparation RG-O/Cu NW hybrid films, first the dispersion of Cu NWs were deposited onto a transparent substrate (mainly onto glass) using a spray-coating method [28]. Density of the Cu NWs on the substrate can be controlled by repeating the pulses of spray coating. After each sprayed pulse, the substrate was kept at 60 °C for about 2 min, and then nitrogen gas was finely blown to the substrate surface to dry completely the sprayed droplets. Figure 5.4a shows the SEM image of the typical spray-coated Cu NW film with random orientation of individual nanowires.

The RG-O can be obtained by depositing and subsequently reducing the G-O films produced. For this, first the graphite oxide composed of highly oxidized graphene platelets was produced using a modified Hummers method [23]. Stirring the graphite oxide particles in water for about 3 h, and subsequent sonication in an ultrasonic bath for about 45 min yield aqueous dispersions of G-O. Thin films of G-O can be produced by spin coating the dispersions onto target substrates. The reduction of the G-O films was performed by exposing the films to hydrazine ($N_2H_4 \cdot H_2O$) vapor at 90 °C for 24 h. The further reduction process was done by thermal annealing the films at 400 °C for 1 h at 1 atm pressure of an Ar (95%) + H (5%) gas mixture.

To fabricate RG-O/Cu NW hybrid films the RG-O films were transferred onto Cu NW films using an approach described elsewhere [28]. For this, a thin film of poly (methyl methacrylate) (PMMA) was deposited on top of the RG-O films on glass substrate by spin coating. The obtained PMMA/RG-O film was subsequently put into 1 M NaOH aqueous solution to delaminate the film from the substrate [52]. In order to remove the residual NaOH the delaminated PMMA/RG-O films were washed three times with de-ionized (DI) water, and then transferred on top of Cu NW films. Afterwards, the PMMA layer was removed with acetone, and the obtained RG-O/Cu NW films were put in a tube furnace to anneal at 180 °C for 30 min at 1 atm pressure of an Ar (95%) + H_2 (5%) gas mixture.

Figure 5.5a shows the optical transmittance and sheet resistance of the pure Cu NW and RG-O/Cu NW hybrid films. The Cu NW films with a low density of nanowires on the substrate surfaces have high optical transmittances (at 550 nm of $T_{550} > 95\%$). However the nanowires in such films do not form globally percolated network, and therefore the films are electrically non-conductive. Repeating the spray pulses can increase the density of NWs on the substrate surface and results in the formation of percolated networks yielding electrically conductive films. The average sheet resistance of such Cu NW films with optical transmittance of $T_{550} = 90\%$ is about $R_s = 295 \pm 19.5\ \Omega$/sq.

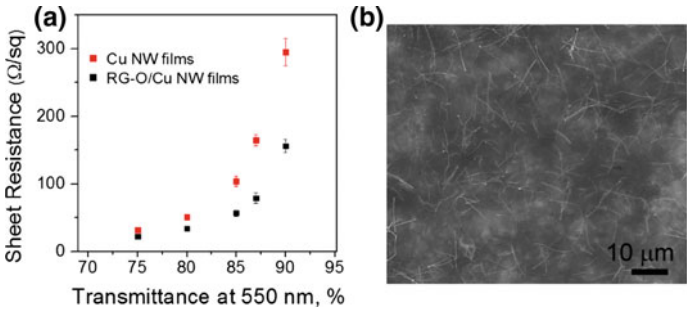

Fig. 5.5 **a** Sheet resistance versus optical transmittance for the pure Cu NW films and RG-O/Cu NW hybrid films. **b** SEM image of a typical RG-O/Cu NW film. Reprinted with permission from [28]. Copyright 2013 American Chemical Society

The RG-O films used in the hybrid films had an average sheet resistance of $R_s = 36.6 \pm 4.7$ kΩ/sq and optical transmittance of $T_{550} = 95.5\%$. The hybrid films had $R_s = 34 \pm 2.6$ Ω/sq at $T_{550} = 80\%$, which is lower than that of pure Cu NW films ($R_s = 51 \pm 4.0$ Ω/sq) and pure RG-O films ($R_s = 7.6 \pm 0.86$ kΩ/sq), each also at $T_{550} = 80\%$. The lower sheet resistance of the hybrid films can be ascribed to Cu NWs that can eliminate or decrease the platelet-platelet junction resistance in the RG-O films, and to the RG-O platelets that can bridge initially non-connected Cu NWs. The RG-O platelets have an average diameter of several micrometers, and can bridge two or more non-connected Cu NWs separated by any distance smaller than the platelet diameter. Figure 5.5b shows that the RG-O platelets cover the empty spaces between NWs providing a continuous 2D platform for charge carriers. Overall, the obtained results demonstrate that the multi-component hybrid films have better optoelectrical characteristics compared to the corresponding single-component films.

In addition to improving the overall conductivity, RG-O platelets can provide additional functionalities. For example, RG-O can act as an oxidation-resistant layer to protect the underneath Cu NWs. Pure Cu NW films are degraded under ambient conditions because of oxidation. Oxidation increases the sheet resistance of the nanowire films, and at higher temperatures this degradation process occurs even faster. The changes of the sheet resistances (R_s) of pure Cu NW and hybrid RG-O/Cu NW films over time in ambient atmosphere at room temperature and at 60 °C are shown in Fig. 5.6a. At room temperature the sheet resistance of the Cu NW films changes from 57 ± 2.5 to 69 ± 3.2 Ω/sq after 72 h. At 60 °C for the same time period the R_s of the nanowire films increases even more rapidly from 56 ± 2.5 to 94 ± 4.7 Ω/sq because of faster oxidation of metal nanowires at elevated temperatures [53]. In contrast, under the same conditions the hybrid films exhibit only minor (in average less than 3% both at room temperature and at 60 °C) changes in R_s. Overall, the minor increase in R_s of the hybrid films compared to that of the pure Cu NW films indicates the higher oxidation-resistance of the hybrid films that can be ascribed to the RG-O layers covering the nanowires.

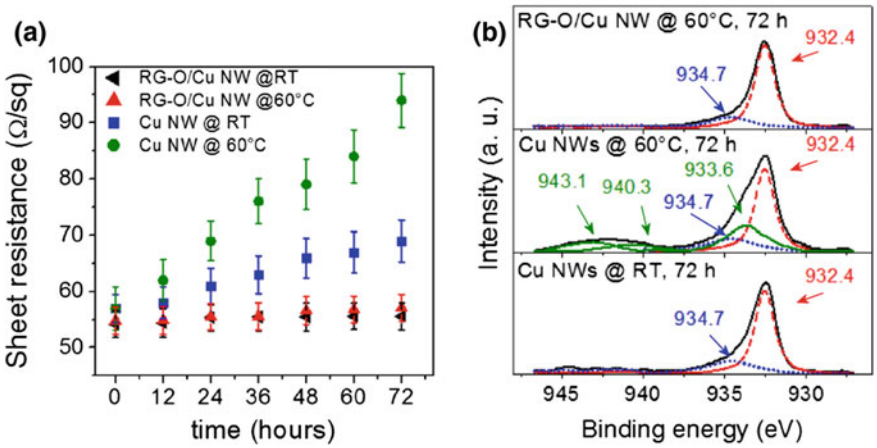

Fig. 5.6 **a** Sheet resistances changes over time for pure Cu NW films and RG-O/Cu NW hybrid films at room temperatures (RT) and at 60 °C. **b** Cu $2p_{3/2}$ XPS spectrum of Cu NW film kept at room temperature (*bottom*), and 60 °C (*middle*) for 72 h, and of RG-O/Cu NW films kept at 60 °C for 72 h (*top*). Reprinted with permission from [28]. Copyright 2013 American Chemical Society

X-ray photoelectron spectroscopy (XPS) studies are consistent with the above shown oxidation-resistance role of RG-O layers in the hybrid films. The high intensity peak (dashed red curve) at ~932.4 eV in the spectrum of the pure Cu NW films kept at room temperature (Fig. 5.6b, bottom spectrum) is ascribed to the overlap of Cu $2p_{3/2}$ and Cu_2O [54] spectral peaks. The low intensity peak (dotted blue curve) at ~934.7 eV is ascribed to $Cu(OH)_2$ [55]. In the spectrum for the Cu NW film kept at 60 °C for 72 h the deconvolution of the peak centered at ~932.4 eV shows the presence of CuO (933.6 eV), $Cu(OH)_2$ (934.7 eV) (dotted blue curve),and the shake-up satellites of CuO (940.3 and 943.1 eV) (solid dark green curves) (Fig. 5.6b, middle spectrum) [54]. The existence of the oxygen containing copper compounds indicate the higher level of oxidation of the Cu NW films compared to the RG-O/Cu NW films (Fig. 5.6b, top spectrum), where such compounds were not observed. These results demonstrate the higher oxidation-resistance of the RG-O/Cu NW hybrid films compared to the pure Cu NW films, and this can be assigned to the RG-O layers that protect the metal nanowires from oxidation.

In the RG-O/Cu NW hybrid films the Cu NWs are considered as the main electrically conductive component. RG-O in this films acts as a multifunctional component simultaneously addressing multiple issues: a continuous film that covers the empty spaces between Cu NWs; a 2D conductive platforma protective layer against oxidation of metal nanowires. Due to these synergistic effects the RG-O/Cu NW hybrid films exhibit higher performance compared to the corresponding single component films.

5.5 CVD-Graphene/Metal Nanowire Hybrid Transparent Conductive Films

CVD-graphene possesses better electrical conductivity compared to RG-O, and therefore it can be main electrically conductive component in the graphene-NW hybrid films. Here, we describe fabrication and optoelectrical properties of CVD-graphene/Ag NW hybrid films with sub-percolation density of Ag NWs. The pure sub-percolated Ag NW films do not form a global network, and therefore the entire film composed of sub-percolated Ag NWs has no electrical conductivity. In the CVD-graphene/Ag NW hybrid films with sub-percolated nanowire components each nanowire can locally contribute with high metallic conductivity to global electrical conductivity of the hybrid films. This allows estimating the contribution of individual metal nanowires (but not the network of NWs) in improving the electrical conductivity of the hybrid films.

CVD-graphene grown on Cu foil can be transferred onto arbitrary substrates using a wet transfer method [18]. Line disruptions in CVD-graphene, as were shown in the SEM images in Fig. 5.3, can be detected by Raman spectroscopy, as well (Fig. 5.7). Presence of defects that cause a double resonance involving transitions around two inequivalent K points of the first Brillouin zone of graphene results in the appearance of the Raman active D mode centered at $\sim$1365 cm^{-1} [56]. Bright lines on the Raman map shown in Fig. 5.7a correspond to the D mode of graphene and can be attributed to the line disruptions. Figure 5.7b shows the individual Raman spectra of graphene taken at areas marked with red, blue and dark cyan circles in the Raman map (Fig. 5.7a). The dark cyan and blue circled areas in the Raman map contain the bright lines (defects), and therefore, the corresponding

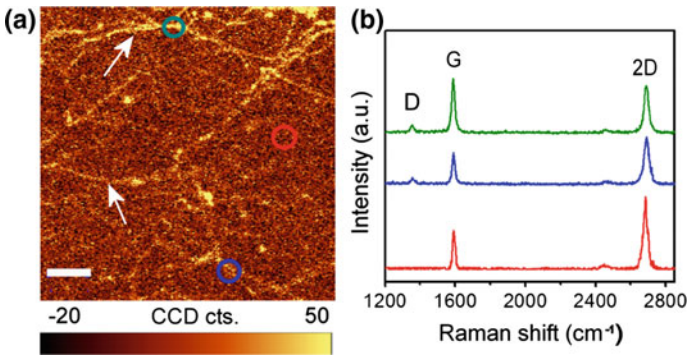

Fig. 5.7 **a** Raman map of CVD-graphene film on a SiO_2/Si substrate (1300–1400 cm^{-1}) around the D mode (1365 cm^{-1}). The line defects (ripples, folding and wrinkles) in the map are shown by the *white arrows*. The scale bar is 10 μm. **b** Raman spectra taken from the areas shown by *red*, *blue* and *dark cyan circles* in the Raman map in (**a**). Raman spectra were taken using WITEC Alpha 300, 100× objective, laser wavelength of 532 nm. Reprinted with permission from [20]. Copyright 2012 American Chemical Society

spectra in Fig. 5.7b show the clearly visible D peaks. Raman spectrum corresponding to the red circled area shows typical CVD-graphene with no observable D peaks. In addition to the D peaks, all three spectra in Fig. 5.7b have relatively high intensity G ($\sim$575 cm^{-1}) and 2D ($\sim$2680 cm^{-1}) peaks. The differences in intensity ratio of G and 2D peaks in blue and dark cyan spectra (I(2D)/I(G) $\approx$ 1.4 for blue, and $\approx$0.9 for dark cyan) indicate the variety of the line disruptions in CVD-graphene. Such transferred CVD-graphene films have a typical sheet resistance of about 1.35 $\pm$ 0.14 kΩ/sq. Thermal annealing at 170 °C for 1 h in a vacuum with a pressure of $p < 2 \times 10^{-2}$ Torr can lower the film sheet resistance to about 1.05 $\pm$ 0.11 kΩ/sq.

Ag NWs (Fig. 5.4b) dispersed in isopropyl alcohol (IPA) (20 mg/ml) was diluted with IPA in order to obtain 0.2, 0.6 and 1.0 mg/mL concentrated Ag NW dispersions. Ag NW films were made by spin coating (3000 rpm) these three dispersions on target substrates, yielding NW films with optical transmittance at 550 nm wavelength (T_{550}) of 98.6, 97.2 and 96.0%, respectively. These films were denoted as NW1, NW2, and NW3, respectively, and all these are non-conductive due to the sub-percolation network of the NWs. Higher (>1.0 mg/mL) concentrations of Ag NW dispersions yield electrically conductive (i.e., percolating) NW films (with $T_{550} < 96\%$), and here we do not consider such films in detail.

To fabricate CVD-graphene/Ag NW hybrid films, CVD-graphene was transferred from the original Cu substrate onto Ag NW films using a double PMMA layer coverage [20]. Figure 5.8a shows a SEM image of the obtained CVD-graphene/Ag NW hybrid films. The graphene layer conforms to the curved surface of the underlying NWs yielding larger contact area between nanowires and graphene layer. This structural feature may improve charge transfer between these two nanostructures resulting in improved conductivity of the hybrid film. The randomly oriented NWs in the hybrid film cross the line disruptions of the graphene (Fig. 5.8b) and can provide 1D pathway for charge transfer.

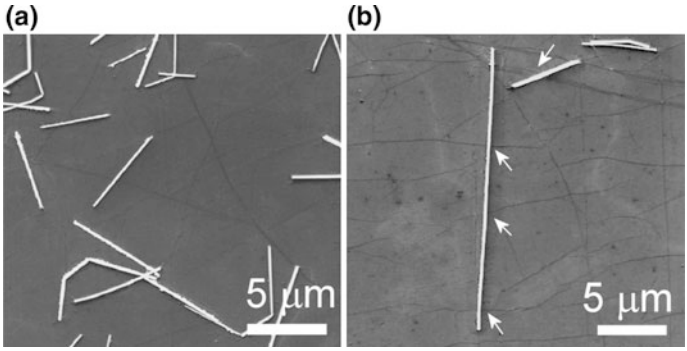

Fig. 5.8 SEM images of **a** a CVD-graphene/Ag NW films, and **b** graphene line disruptions crossing Ag NW shown by *arrows*. Reprinted with permission from [20]. Copyright 2012 American Chemical Society

Figure 5.9a shows the optical transmittance of CVD-graphene and CVD-graphene/Ag NW hybrid films with transparency of >90% in the presented spectral region (400–1000 nm). Optical transmittance vesus the R_s of the films measured after annealing at 170 °C for 1 h in a vacuum with a pressure of $p < 2 \times 10^{-2}$ Torr is depicted in Fig. 5.9b. The sheet resistance of the CVD-graphene/Ag NW films depends on the density of the Ag NWs. The CVD-graphene/NW3 films have the lowest sheet resistance $R_s = 64 \pm 6.1$ Ω/sq with $T_{550} = 93.6\%$ that is comparable to the values (30 Ω/sq for CVD-graphene/SiO_2 system) theoretically predicted for appropriately doped 'perfect' graphene when solely electron-phonon scattering is considered [40]. Such greatly improved conductivity of the hybrid films compared to pure typical CVD-graphene films ($R_s = 1.05 \pm 0.11$ kΩ/sq) can be ascribed to the Ag NWs that provide metallic 1D conductivity pathways. In these hybrid films, graphene is the main conductive component while Ag NWs contribute only locally because of their sub-percolation density.

Further decrease in the sheet resistance of the hybrid films can be achieved by increasing the density of Ag NWs or by adding another layer of graphene. For example, adding a second graphene layer onto the CVD-graphene/NW3 allows decreasing the films sheet resistance to about 24 (±3.6) Ω/sq with $T_{550} \approx 91\%$ (CVD-graphene × 2/NW3 in Fig. 5.9b).

In the presented CVD-graphene/sub-percolated Ag NW films the graphene layer is the main globally conductive component while Ag NWs are an additional component (globally non-conductive) that can locally contribute to the conductivity of the hybrid films. Using percolated NW films or metal grids yields hybrid films with further enhanced conductivities, as has been demonstrated recently [21, 57]. In such films metal structures are considered as main conductive components.

As in case of RG-O layer in RG-O/Cu NW hybrid films, demonstrated in the previous section, graphene in CVD-graphene/Ag NW hybrid films can also provide additional functionalities resulting in improved performance of the hybrid films.

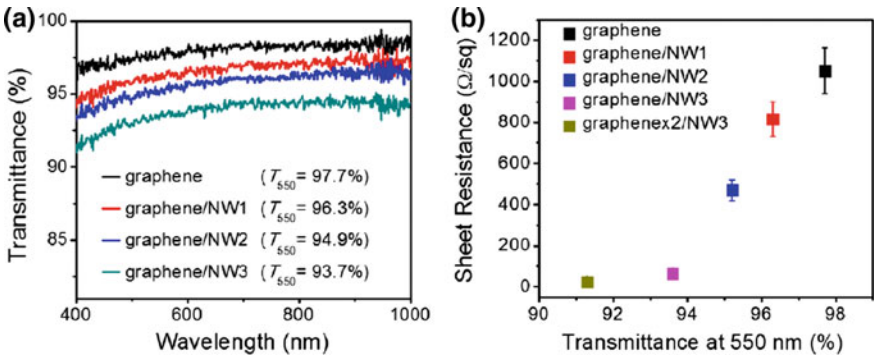

Fig. 5.9 **a** Optical transmittance of CVD-graphene and CVD-graphene/Ag NW films. **b** Sheet resistance versus optical transmittance for CVD-graphene and CVD-graphene/Ag NW films. Reprinted with permission from [20]. Copyright 2012 American Chemical Society

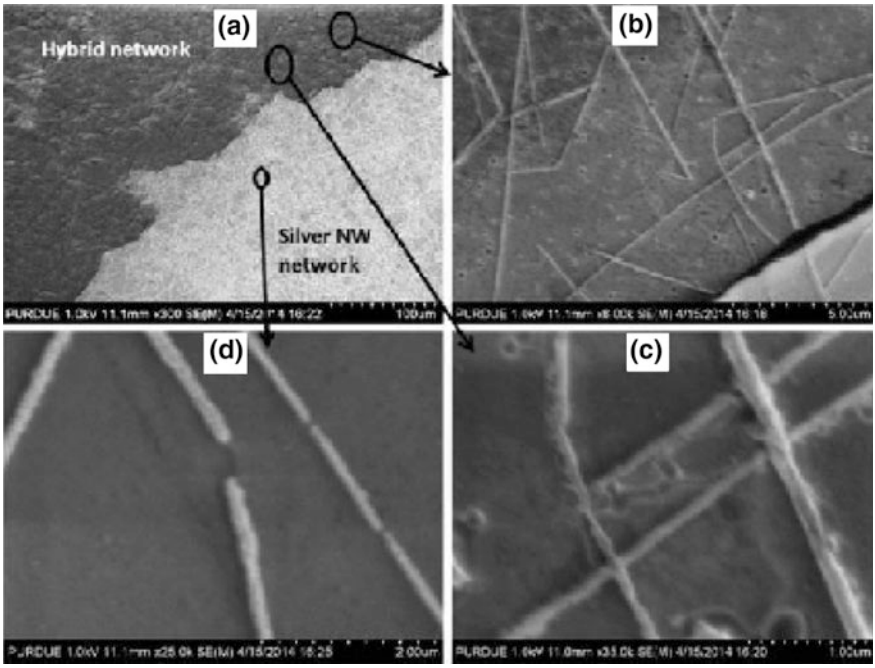

Fig. 5.10 SEM of silver nanowires after laser irradiation with intensity of 0.8 MW cm^{-2}: **a** A comparison between NW network region and hybrid NW network region (note the difference in the image contrast between the two regions). **b**, **c** High-magnification SEM images of two randomly located hybrid network regions. **d** High-magnification SEM view of a representative randomly located nanowire network region. Reprinted with permission from [51]. Copyright 2015 American Chemical Society

One of such functionalities of graphene, namely the protection of Ag NWs from harsh radiation environment has been recently studied [51]. For these studies thin films of CVD-graphene/Ag NWs (darker area in Fig. 5.10a) and pure Ag NWs (lighter area in Fig. 5.10a) were exposed to intense 248 nm KrF excimer laser beams with nanosecond pulses widths and with varied laser intensities corresponding to millions of W cm^{-2} power densities. It was demonstrated that after exposing to the laser beam the Ag NWs covered with graphene layer were not damaged (Fig. 5.10b, c), while the uncovered Ag NWs deformed, converted into nanosegments (Fig. 5.10d), and eventually into nanobeads along the length of the nanowires. In the CVD-graphene/Ag NW films, the graphene layer extracts and spreads the most of the thermal energy from the nanowires to the graphene lattice, thereby protecting the nanowires from thermal damaging. This functionality of the graphene layer enables using the hybrid films at elevated temperatures for longer terms compared to the pure Ag NW films.

It should be noted that the electromechanical performance of the hybrid films is another major advantage over ITO. Although all RG-O/Cu NW and CVD-graphene/Ag

NW hybrid films presented above were on rigid substrates, similar optoelectrical results for the films deposited on flexible substrates can be obtained because all thin film fabrication and processing are compatible with flexible substrates. In addition, excellent stability of numerous graphene/metal NW hybrid films under mechanical strains has been reported in recent literatures [34, 57, 58].

5.6 Applications of Graphene/Metal Nanowire Hybrid Films

As shown above, the hybrid films composed of RG-O or CVD-graphene and metal nanowires have a great potential for TCF applications due to their optoelectrical characteristics. The hybrid films have been recently tested in diverse optoelectronic devices, such as CdTe solar cells [59], light emitting diodes [60], single-pixel contact lenses [57] showing feasibility of the films as transparent electrodes in these devices. Some applications of the hybrid films have been summarized in recent literature [61]. Here, we show two examples of the applications of RG-O/Cu NW and CVD-graphene/Ag NW hybrid films as transparent electrodes in electrochromic (EC) devices. Using two different EC cells we highlight two different aspects of the hybrid films: (i) better performance of the hybrid TCF compared to single component NW TCFs, and (ii) hybrid TCFs can replace the conventional ITO in EC devices.

5.6.1 Application of RG-O/Cu NW Transparent Electrodes in EC Devices

Working principle of EC devices is based on the reversible change the optical properties of the EC material induced by an external electric field. These devices can be used for diverse applications, including displays, gas sensors, antiglare mirrors and smart windows. The latter application represents an important use to shadow buildings against direct solar radiation to reduce the heat load, and in majority cases requires large-area device fabrication. Below we provide more detailed description of EC device fabrication steps using the hybrid films as transparent electrodes. Most aspects of the fabrication of electrochromic devices can be applied for sandwich-structured optoelectronic devices, such as dye-sensitized solar cells and OLEDs.

The RG-O/Cu NW hybrid films were tested as transparent electrodes in Prussian blue (PB)-based electrochromic (EC) devices. This kind of EC device typically consists of a thin PB film deposited onto a transparent electrode, usually ITO. Here, RG-O/Cu NW hybrid films on glass substrates were used to replace ITO electrodes [28]. An aqueous solution of 0.05 M hydrochloric acid (HCl), 0.05 M iron(III)

chloride ($FeCl_3$), and 0.05 M potassium hexacyanoferrate (III) ($K_3[Fe(CN)_6]$) in a 1:2:2 ratio was used to electrochemically deposit PB films onto the RG-O/Cu NW transparent electrodes [62]. PB films with homogeneous thicknesses on top of the RG-O/Cu NW electrode can be obtained by applying a voltage to the RG-O/Cu NW electrode and Pt counter electrode, both immersed into the solution [63].

An external electric voltage applied to the RG-O/Cu NW transparent electrode of the EC device and the Pt counter electrode (Fig. 5.11a) induces an electrochemical reaction that results in reversible modulations of optical characteristics of PB layers. Electrochemical reduction of the PB layer converts a mixed-valence (Fe^{2+}, Fe^{3+}) compound into a single-valence (Fe^{2+}) compound (and vice versa upon oxidation) and changes the color of the PB layer from blue to colorless (from colorless to blue upon oxidation). This electrochemical reaction can be described as [63]:

$$(\text{blue})\ Fe_4^{3+}\left[Fe^{2+}(CN)_6\right]_3 + 4\,K^+ + 4e^- \Leftrightarrow (\text{colorless})\ K_4Fe_4^{2+}\left[Fe^{2+}(CN)_6\right]_3$$

The redox reactions leading to the coloration/bleaching of PB-based EC devices can be simply carried out using 1 M KCl aqueous solution as an electrolyte (Fig. 5.11a). Bleached colorless state of the EC device can be obtained by applying an external voltage (−0.6 V) to the RG-O/Cu NW TCF, and the blue colored state is achieved by applying a reverse external field. Figure 5.11b shows the optical transmittance spectra of the PB layer at the bleached (T_{550} = 79.2%) and colored (T_{550} = 36.4%) states. Typical times needed for the bleached-to-colored and colored-to-bleached processes in the tested EC devices are measured to be 75 and 95 s, respectively, which are similar to that of a PB EC device with an ITO electrode [62, 63].

In contrast the RG-O-Cu NW hybrid films, pure Cu NW transparent electrodes cannot work in the PB EC devices. This has been demonstrated using a two-area

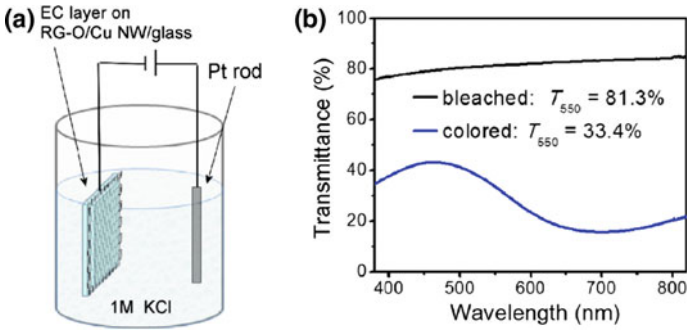

Fig. 5.11 **a** Schematic of an EC device with a PB layer deposited onto the RG-O/Cu NW electrode and Pt rod used as a counter electrode, both immersed into an electrolyte. **b** Optical transmittance of colored and bleached PB films deposited on a RG-O/Cu NW transparent electrode. Reprinted with permission from [28]. Copyright 2013 American Chemical Society

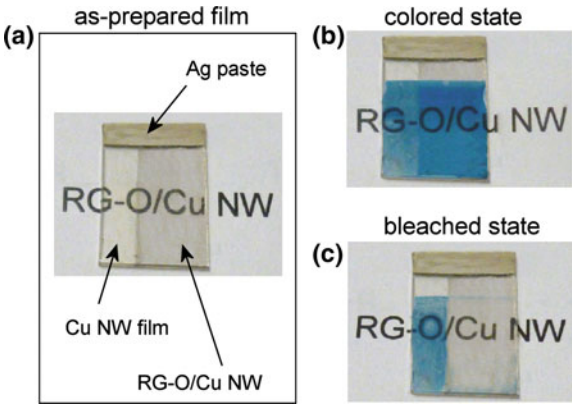

Fig. 5.12 Digital photograph of **a** as-prepared two-area transparent electrode with areas covered by a pure Cu NW film and a hybrid RG-O/Cu NW film, as shown by the *arrows* (*left*). PB EC layer on the two-area electrode **b** after coloration, and **c** bleaching processes. Reprinted with permission from [28]. Copyright 2013 American Chemical Society

transparent electrode (a glass substrate with one-half covered by RG-O/Cu NW hybrid film and the other by pure Cu NW film, as shown in Fig. 5.12a). After deposition of a PB layer onto this electrode, entire surface of the electrode has been homogeneously colored (Fig. 5.12b, colored state). In electrochemical bleaching, the PB layer deposited on the RG-O/Cu NW hybrid film has been bleached, while no bleaching of the PB on top of the pure Cu NW film occurred (Fig. 5.12c, bleached state). This can be explained by the fact that during the deposition of PB layers pure Cu NWs reacted with PB forming copper hexacyanoferrate compounds [64]. This reaction destroys the Cu NW network(s), the area of the electrode initially covered with pure Cu NWs has no electrical conductivity. In addition, immersing the electrode into the electrolyte solution leads to partial delamination of the Cu NWs from the electrode area covered with the pure Cu NW film, which also results in worsening the electrical conductivity of the pure Cu NW films. In contrast, the PB layer, deposited onto the electrode area covered with RG-O/Cu NW films, can be repeatedly electrochemically colored and bleached. This indicates that the RG-O platelets in RG-O/Cu NW films protect the Cu NWs from reacting with the PB layer. Also, no delamination of Cu NWs from the electrode area covered with RG-O/Cu NW film was observed.

The presented example demonstrates that RG-O/Cu NW hybrid films exhibit better performance compared to pure Cu NWs. However, it should be noted that lowering the RG-O thickness and/or increasing the cycling results in gradual degradation of RG-O/Cu NW hybrid films in the EC device. These observations indicate that currently, the nanostructured hybrid TCFs can be selectively used in certain type of devices, and further improvement is needed in order to expand their use in wider range of optoelectronic applications. In addition to the optical, electrical and mechanical properties of the hybrid films, their long-term use and material consistencies/inconsistencies of the hybrid films needs to be more rigorously studied.

5.6.2 Application of CVD-Graphene/Ag NW Transparent Electrodes in EC Devices

CVD-graphene/Ag NW films were used as a transparent electrode in another EC device with an electrochromic WO_3 layer [20]. This kind of EC devices consist of an EC thin film and an electrolyte layer sandwiched between two transparent electrodes (usually ITO electrodes). An external voltage applied to the electrodes can modulate the optical characteristics of the EC layer [65, 66]. Here, the CVD-graphene/Ag NW films on glass substrates were used to replace one of the two ITO TCFs as shown in Fig. 5.13a. Nanostructured sol-gel synthesized WO_3 films that exhibit improved performance of EC devices with fast coloration/bleaching kinetics were chosen as the EC layer [65–67]. However, direct spin-coating of sol-gel synthesized WO_3 onto CVD-graphene/Ag NW hybrid films with no buffer layer yields EC films with non-uniform thicknesses and inhomogeneous morphologies. Therefore, first, using thermal evaporation of WO_3 powder, a buffer layer—100 nm thick WO_3 film was deposited onto the CVD-graphene/Ag NW electrode. This buffer layer provides a good surface for spin coating of sol–gel prepared nanostructured WO_3 films onto it. The total thickness of the double layer WO_3 thin films with highly porous surface structure (Fig. 5.13b) was about 500 nm. A propylene/ethylene carbonate solution (1:1) containing 1 M $LiClO_4$ was chosen as a Li-conductive electrolyte. Figure 5.13a shows the schematic of complete EC device with WO_3 EC layers and electrolyte sandwiched between ITO and CVD-graphene/Ag NW transparent electrodes deposited on glass substrates.

An external voltage applied to the electrodes (3.0 V, negative to the CVD-graphene/Ag NW and positive to the ITO) induces the injection of electrons and intercalation of Li^+ cations into the WO_3 films and yields W^{+5} sites. Subsequently the charge transfer between the W^{+6} and W^{+5} states occurs in the WO_3 films. This process is accompanied with strong optical absorption leading to blue coloration of the WO_3 layers. The reaction is described as [66]:

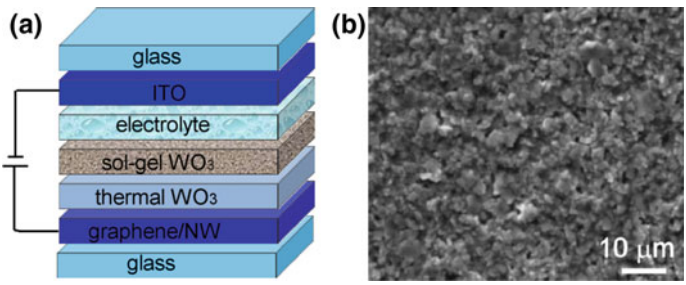

Fig. 5.13 **a** Schematic of an EC device. Reprinted with permission from [20]. Copyright 2012 American Chemical Society. **b** SEM image of double layer WO_3 film deposited onto CVD-graphene/Ag NW transparent conductive electrode

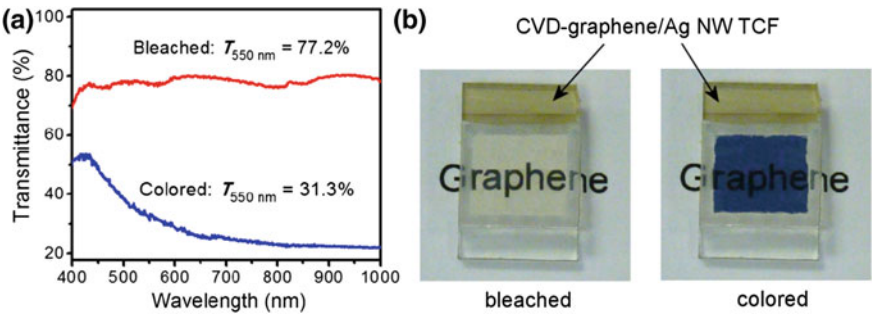

Fig. 5.14 **a** Optical transmittance spectra of the EC device in bleached and colored states. **b** Digital photographs of the bleached and colored EC devices with a background "Graphene". A conductive silver paste (*yellow area*) on top of the CVD-graphene/Ag NW electrode was used to improve the electrical contacts. Reprinted with permission from [20]. Copyright 2012 American Chemical Society

$$WO_3 + x[Li^+ + e^-] \rightarrow Li_xW^{+6}_{(1-x)}W^{+5}_x O^3,$$

where x is the fractional number of WO_3 lattice sites filled with Li cations. Extraction of Li^+ ions from the WO_3 layers and bleaching the EC film can be obtained by applying a reverse external voltage to the electrodes. Typical optical transmittance of the EC device in bleached (T_{550} = 77.2%) and colored (T_{550} = 31.3%) states is shown in Fig. 5.14a.

The photographs of the EC device in bleached and colored states are shown in Fig. 5.14b. The stable times of 115 and 205 s for 90% optical transmittance change from bleached-to-colored and from colored-to-bleached states, respectively are obtained after several initial coloration/bleaching cycles. These values are similar to that of a EC device with the same electrolyte and sol–gel EC film, but using two ITO electrodes [67].

The presented applications of the hybrid films in the EC devices demonstrate the feasibility of the graphene/metal NW hybrid films for TCF applications. Further research studies and optimization of properties of the hybrid films are needed to accelerate the practical application of graphene-metal nanowire hybrid films in various optoelectronic devices including displays, touch screens, solar cells, OLEDS, electromagnetic shielding and transparent heaters.

5.7 Conclusions and Future Challenges

Commercially available ITO transparent conductive films cannot meet the performance metrics of new TCF-based devices, especially in emerging technologies such as flexible displays, solar cells, transistors, sensors and energy storage systems. Hybrid films composed of two or more components not only exhibit better

performance compared to that of the corresponding single component films, but also they possess optical, electrical and mechanical properties similar or superior to that of conventionally used transparent oxide conductors.

The strategy to assemble 1D metal NWs and 2D graphene films allows one to obtain hybrid films with excellent control of nanoscale morphology, where the limitation of one component is compensated by the strengths of the other component. In terms of the two main TCF characteristics: optical transmittance and electrical conductivity, the hybrid films are comparable to or better than ITO films. Another advantage of the hybrid films over ITO films is their good electromechanical stabilities that make them suitable for flexible optoelectronic devices. Overall, the strategy to fabricate the hybrid films not only allows replacing ITO films, but also can provide a path to next generation TCFs with novel architectures and additional functionalities.

In spite of these advantages, today, the hybrid films have not yet fully expanded in the market to replace the ITO films in the existing and emerging optoelectronic device applications. The successful realization of a great potential of the hybrid films requires extensive investigation and comprehensive analysis of both fundamental and application-specific characteristics of the hybrid films. Furthermore, research and development addressing the following issues: (i) developing of advanced methods for fabrication of high-quality, low-cost and large-scale hybrid films; (ii) thermal, chemical, environmental stability of the films, (iii) optimization of compositional and structural performance, (iv) designing and assembling of components, and integration testing of hybrid films in a broad range of devices are vitally important to realize the potential of the hybrid transparent conductive films. In addition, to improve the feasibility of the hybrid films for practical applications, it is important to test the compatibility of the hybrid films with active parts of diverse optoelectronic devices, and studying, detecting and eliminating the film performance issues for long-term applications.

Acknowledgements Dr. Kholmanov thanks Prof. R. Ruoff for his collaboration, and would like to acknowledge the support from Tokyo Electron Ltd.—customized Semiconductor Research Corporation (Project#2009-OJ-1873). Prof. Alam will like to acknowledge his long term collaborations: Prof. D. Janes, Prof. J. Rogers, Prof. Shakouri, Dr. S. Das, Dr. R. Chen, Dr. C. Jeong. The work was supported by Semiconductor Research Corporation (Project # 2009-OJ-1873) and National Science Foundation Grant ECCS 1408346. Prof. Sberveglieri would like to acknowledge the support from European Union Research and Innovation Funding Program FP7 (Project# FP7-ICT-2013-10).

References

1. K. Ellmer, Nat. Photonics **6**, 9 (2012)
2. D.S. Hecht, L. Hu, G. Irvin, Adv. Mater. **23**, 1482 (2011)
3. T. Minami, Semicond. Sci. Technol. **20**, S35 (2005)
4. S.T. Lee, Z.Q. Gao, L.S. Hung, Appl. Phys. Lett. **75**, 1404 (1999)

5. M.P. de Jong, D.P.L. Simons, M.A. Reijme, L.J. van Ijzendoorn, A.W. Denier van der Gon, M.J.A. de Voigt, H.H. Brongersma, R.W. Gymer, Synth. Met. **110**, 1 (2000)
6. M. Jørgensen, K. Norrman, S.A. Gevorgyan, T. Tromholt, B. Andreasen, F.C. Krebs, Adv. Mater. **24**, 580 (2012)
7. S. Savagatrup et al., Energy Environ. Sci. **8**, 55 (2015)
8. M.G. Kang, L.J. Guo, Adv. Mater. **19**, 1391 (2007)
9. M. Zhang, S. Fang, A.A. Zakhidov, S.B. Lee, A.E. Aliev, C.D. Williams, K.R. Atkinson, R. H. Baughman, Science **309**, 1215 (2005)
10. F. Mirri, A.W.K. Ma, T.T. Hsu, N. Behabtu, S.L. Eichmann, C.C. Young, D.E. Tsentalovich, M. Pasquali, ACS Nano **6**, 9737 (2012)
11. Q. Cao, J.A. Rogers, Adv. Mater. **21**, 29 (2009)
12. N. Pimparkar, M.A. Alam, IEEE Electron Device Lett. **29**, 1037 (2008)
13. S.V. Morozov, K.S. Novoselov, M.I. Katsnelson, F. Schedin, D.C. Elias, J.A. Jaszczak, A.K. Geim, Phys. Rev. Lett. **100**, 016602 (2008)
14. A.B. Kuzmenko, E. van Heumen, F. Carbone, D. van der Marel, Phys. Rev. Lett. **100**, 117401 (2008)
15. R.R. Nair, P. Blake, A.N. Grigorenko, K.S. Novoselov, T.J. Booth, T. Stauber, N.M.R. Peres, A.K. Geim, Science **320**, 1308 (2008)
16. Q. Zheng, Z. Li, J. Yang, J.-K. Kim, Prog. Mater Sci. **64**, 200 (2014)
17. H.A. Becerril, J. Mao, Z. Liu, R.M. Stoltenberg, Z. Bao, Y. Chen, ACS Nano **2**, 463 (2008)
18. X. Li, Y. Zhu, W. Cai, M. Borysiak, B. Han, D. Chen, R.D. Piner, L. Colombo, R.S. Ruoff, Nano Lett. **9**, 4359 (2009)
19. C. Jeong, P. Nair, M. Khan, M. Lundstrom, M.A. Alam, Nano Lett. **11**, 5020 (2011)
20. I.N. Kholmanov et al., Nano Lett. **12**, 5679 (2012)
21. Y. Zhu, Z. Sun, Z. Yan, Z. Jin, J.M. Tour, ACS Nano **5**, 6472 (2011)
22. W.S. Hummers, R.E. Offeman, J. Am. Chem. Soc. **80**, 1339 (1958)
23. S. Stankovich, D.A. Dikin, G.H.B. Dommett, K.M. Kohlhaas, E.J. Zimney, E.A. Stach, R.D. Piner, S.T. Nguyen, R.S. Ruoff, Nature **442**, 282 (2006)
24. X. Wang, L. Zhi, K. Müllen, Nano Lett. **8**, 323 (2008)
25. V. Galstyan, E. Comini, I. Kholmanov, G. Faglia, G. Sberveglieri, Rsc Adv. **6**, 34225 (2016)
26. I.N. Kholmanov et al., ACS Nano **6**, 5157 (2012)
27. S. Gilje, S. Han, M. Wang, K.L. Wang, R.B. Kaner, Nano Lett. **7**, 3394 (2007)
28. I.N. Kholmanov et al., ACS Nano **7**, 1811 (2013)
29. H.-J. Shin et al., Adv. Func. Mater. **19**, 1987 (2009)
30. M. Zhou, Y. Wang, Y. Zhai, J. Zhai, W. Ren, F. Wang, S. Dong, Chemistry. Eur J **15**, 6116 (2009)
31. Y. Shao, J. Wang, M. Engelhard, C. Wang, Y. Lin, J. Mater. Chem. **20**, 743 (2010)
32. Z.-J. Fan, W. Kai, J. Yan, T. Wei, L.-J. Zhi, J. Feng, Y.-M. Ren, L.-P. Song, F. Wei, ACS Nano **5**, 191 (2011)
33. X. Mei, J. Ouyang, Carbon **49**, 5389 (2011)
34. S.H. Domingues et al., Carbon **63**, 454 (2013)
35. X. Wang, I. Kholmanov, H. Chou, R.S. Ruoff, ACS Nano **9**, 8737 (2015)
36. X. Li et al., Science **324**, 1312 (2009)
37. S. Bae et al., Nat Nano **5**, 574 (2010)
38. X. Du, I. Skachko, A. Barker, E.Y. Andrei, Nat Nano **3**, 491 (2008)
39. G.-X. Ni et al., ACS Nano **6**, 1158 (2012)
40. J.-H. Chen, C. Jang, S. Xiao, M. Ishigami, M.S. Fuhrer, Nat Nano **3**, 206 (2008)
41. P.Y. Huang et al., Nature **469**, 389 (2011)
42. O.V. Yazyev, S.G. Louie, Nat. Mater. **9**, 806 (2010)
43. I.N. Kholmanov, J. Edgeworth, E. Cavaliere, L. Gavioli, C. Magnuson, R.S. Ruoff, Adv. Mater. **23**, 1675 (2011)
44. S. Karoui, H. Amara, C. Bichara, F. Ducastelle, ACS Nano **4**, 6114 (2010)
45. Q. Yu et al., Nat. Mater. **10**, 443 (2011)
46. L. Hu, H.S. Kim, J.-Y. Lee, P. Peumans, Y. Cui, ACS Nano **4**, 2955 (2010)

47. A.R. Rathmell, B.J. Wiley, Adv. Mater. **23**, 4798 (2011)
48. D.-S. Leem, A. Edwards, M. Faist, J. Nelson, D.D.C. Bradley, J.C. de Mello, Adv. Mater. **23**, 4371 (2011)
49. E.C. Garnett, W. Cai, J.J. Cha, F. Mahmood, S.T. Connor, M. Greyson Christoforo, Y. Cui, M.D. McGehee, M.L. Brongersma, Nat. Mater. **11**, 241 (2012)
50. H. Wu et al., Nat Nano **8**, 421 (2013)
51. S.R. Das, Q. Nian, M. Saei, S. Jin, D. Back, P. Kumar, D.B. Janes, M.A. Alam, G.J. Cheng, ACS Nano **9**, 11121 (2015)
52. H. Yamaguchi, G. Eda, C. Mattevi, H. Kim, M. Chhowalla, ACS Nano **4**, 524 (2010)
53. A.R. Rathmell, M. Nguyen, M. Chi, B.J. Wiley, Nano Lett. **12**, 3193 (2012)
54. C.-K. Wu, M. Yin, S. O'Brien, J.T. Koberstein, Chem. Mater. **18**, 6054 (2006)
55. C.E. Dubé, B. Workie, S.P. Kounaves, A. Robbat, M.L. Aksub, G. Davies, J. Electrochem. Soc. **142**, 3357 (1995)
56. A.C. Ferrari, Solid State Commun. **143**, 47 (2007)
57. M.-S. Lee et al., Nano Lett. **13**, 2814 (2013)
58. B. Deng et al., Nano Lett. **15**, 4206 (2015)
59. J. Liang, H. Bi, D. Wan, F. Huang, Adv. Func. Mater. **22**, 1267 (2012)
60. J. Liang, L. Li, K. Tong, Z. Ren, W. Hu, X. Niu, Y. Chen, Q. Pei, ACS Nano **8**, 1590 (2014)
61. R. Das Suprem, S. Sadeque, C. Jeong, R. Chen, A. Alam Muhammad, B. Janes David, Nanophotonics, 180 (2016)
62. S. Lupu, C. Mihailciuc, L. Pigani, R. Seeber, N. Totir, C. Zanardi, Electrochem. Commun. **4**, 753 (2002)
63. A.A. Karyakin, Electroanalysis **13**, 813 (2001)
64. O. Makowski, J. Stroka, P.J. Kulesza, M.A. Malik, Z. Galus, J. Electroanal. Chem. **532**, 157 (2002)
65. M. Deepa, A.K. Srivastava, M. Kar, S.A. Agnihotry, J. Phys. D Appl. Phys. **39**, 1885 (2006)
66. P.R. Somani, S. Radhakrishnan, Mater. Chem. Phys. **77**, 117 (2003)
67. A.E. Aliev, H.W. Shin, Solid State Ionics **154–155**, 425 (2002)